

**PROTON-PROTON, PION-PROTON AND PION-PION
DIFFRACTIVE COLLISIONS AT ULTRA-HIGH ENERGIES**

V.V. ANISOVICH

*National Research Centre "Kurchatov Institute", Petersburg Nuclear Physics Institute, Gatchina
188300, Russia*

K.V. NIKONOV

*National Research Centre "Kurchatov Institute", Petersburg Nuclear Physics Institute, Gatchina
188300, Russia*

V.A. NIKONOV

*National Research Centre "Kurchatov Institute", Petersburg Nuclear Physics Institute, Gatchina
188300, Russia*

J. NYIRI

Institute for Particle and Nuclear Physics, Wigner RCP, Budapest 1121, Hungary

The LHC energies are those at which the asymptotic regime in hadron-hadron diffractive collisions ($pp, \pi p, \pi\pi$) might be switched on. Based on results of the Dakhno-Nikonov eikonal model which is a generalization of the Good-Walker eikonal approach for a continuous set of channels, we present a picture for transformation of the constituent quark mode to the black disk one. In the black disk mode ($\sqrt{s} \geq 10$ TeV) we have a growth of the logarithm squared type for total and elastic cross sections, $\sigma_{tot} \sim \ln^2 s$ and $\sigma_{el} \sim \ln^2 s$, and ($\tau = \mathbf{q}_\perp^2 \sigma_{tot}$)-scaling for diffractive scattering and diffractive dissociation of hadrons. The diffractive dissociation cross section grows as $\sigma_D \sim \ln s$, $\sigma_{DD} \sim \ln s$, and their relative contribution tends to zero: $\sigma_D/\sigma_{tot} \rightarrow 0$, $\sigma_{DD}/\sigma_{tot} \rightarrow 0$. Asymptotic characteristics of diffractive and total cross sections are universal, and this results in the asymptotical equality of cross sections for all types of hadrons (the Gribov's universality). The energy scale for switching on the asymptotic mode is estimated for different processes.

PACS numbers: 13.85.-t 13.75.Cs 14.20.Dh

The observation of the total cross section growth at pre-LHC energies, $\sqrt{s} \sim 0.2 - 1.8$ TeV,¹⁻⁵ initiates studies of corresponding models such as that with an increase allowed by the Froissart bound⁶ or exceeding it, for example, by the power- s behavior.^{7,8} The necessity of the s -channel unitarization of scattering amplitudes actualizes the use of the Glauber approach.^{9,10} On account of the s -channel rescatterings, the power- s growth of amplitudes is dampened to the $(\ln^2 s)$ -type, see 11, 12, 13. Still, let us emphasize, exceeding the Froissart bound does not violate general constraints for the scattering amplitude.¹⁴

Recent measurements at LHC (ATLAS,¹⁵ CMS,¹⁶ TOTEM¹⁷ collaborations)

and cosmic ray data¹⁸ initiate further interest to s -channel unitarized amplitudes, see, for example, 19, 20, 21, 22, 23, 24, 25, 26, 27, 28, 29, 30.

1. Diffractive Hadron-Hadron Scattering in the Dakhno-Nikonov Eikonal Model

A model for high-energy πp and $p^\pm p$ collisions with the eikonal unitarization of scattering amplitudes was suggested by Dakhno and Nikonov³¹ and successfully used for the description of the pre-LHC data. The model takes into account the quark structure of colliding hadrons, the gluon origin of the input pomeron and the colour screening effects in collisions. The model can be considered as a version of the Good-Walker eikonal approach³² for a continuous set of channels.

The extension of the Dakhno-Nikonov model to LHC energies was carried out in 33 for diffractive pp -scattering. The pp data were re-fitted taking into account new results in the TeV-region.^{17, 18} The region 5-50 TeV turns out to be that where the asymptotics starts. It means that the asymptotic regime should reveal itself definitely at $10^2 - 10^4$ TeV; an analysis of the diffractive cross sections at ultrahigh energies was carried out in 34. The total and elastic hadron-hadron cross sections are approaching the asymptotic values ($\sigma_{tot}^\sim(s)$ and $\sigma_{el}^\sim(s)$) from bottom to top:

$$\begin{aligned} \sigma_{tot}(s) &\sim \ln^2 s, & \sigma_{el}(s) &\sim \ln^2 s, \\ \left[\frac{\sigma_{el}(s)}{\sigma_{tot}(s)} \right]_{\ln s \rightarrow \infty} &\rightarrow \frac{1}{2}, & \frac{\sigma_{tot}(s)}{\sigma_{tot}^\sim(s)} &< 1, & \frac{\sigma_{el}(s)}{\sigma_{el}^\sim(s)} &< 1, \end{aligned} \quad (1)$$

that gives the illusion of exceeding the Froissart bound (see, for example, the discussion in 35, 36).

Further, the model predicts that differential elastic cross sections depend asymptotically on transverse momenta with a relation for τ -scaling:

$$\begin{aligned} \frac{1}{\sigma_{tot}(s)} \frac{d\sigma_{el}(\tau)}{d\tau} &= D(\tau), & \int_0^\infty d\tau D(\tau) &= \frac{\sigma_{el}(s)}{\sigma_{tot}(s)}, \\ \tau &= \mathbf{q}_\perp^2 \sigma_{tot} \propto \mathbf{q}_\perp^2 \ln^2 s, \end{aligned} \quad (2)$$

where τ and $D(\tau)$ are dimensionless variables. In pp collision the τ -scaling is working for $1/\sigma_{tot} \times d\sigma_{el}/d\tau$ within 10% accuracy for $0 < \tau < 4$ at $\sqrt{s} \simeq 10$ TeV, and for $\sqrt{s} \simeq 100$ TeV this region is extended to $0 < \tau < 10$.

The model points to the universal behaviour of all total cross sections (the Gribov universality³⁷). It is the consequence of the universality of the colliding disk structure (or the structure of parton clouds) at ultrahigh energies. The question is at what energy range the asymptotic modes are switched on for different processes.

Slow switching on of the asymptotic regime in the hadron diffractive collisions is related both to the twofold structure of hadrons (hadrons are built by constituent quarks and the latter are formed by clouds of partons) and the gluon origin of the pomeron. In the impact parameter space the parton clouds fill first the intrinsic

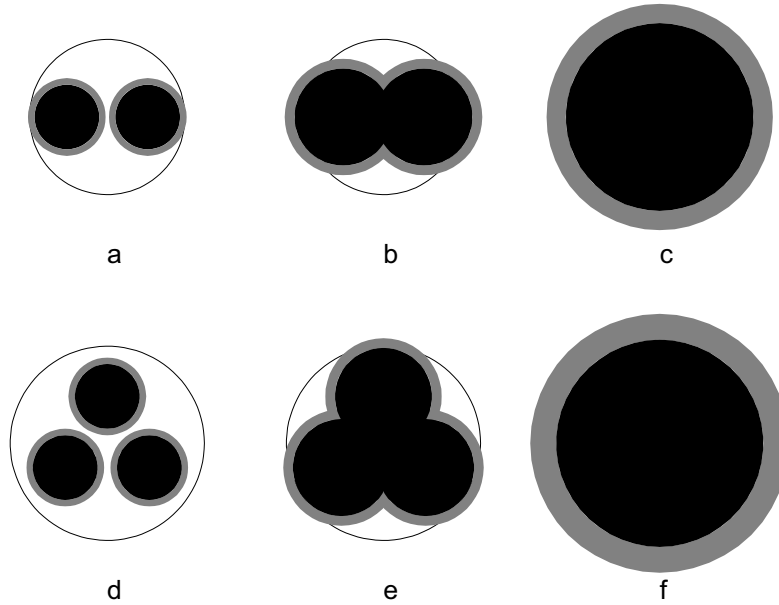


Fig. 1. Meson and proton pictures in the impact parameter space at moderately high energies (a,d) and their transformations with increasing energy (b,e) to ultrahigh region where universal black disks are created (c,f).

hadron domain, see Figs. 1a,d for pion and proton. At ultra-high energies the situation is transformed to a one-disk picture, Figs. 1c,f that manifests itself in two-step asymptotics. The energy of this transformation is that of LHC, Figs. 1b,e.

The calculations we have carried out demonstrate a comparatively fast approach of $\sigma_{tot}(s)$ to the asymptotic behavior being in contrast to $\sigma_{el}(s)$. The slow increase of $\sigma_{el}(s)$ means a slow approach of $\sigma_{inel}(s) = \sigma_{tot}(s) - \sigma_{el}(s)$ to the asymptotic mode.

A fast approach to the asymptotic mode is observed for the sum of elastic and quasi-elastic cross sections (elastic, single diffractive dissociations and double diffractive dissociation). That emphasizes the importance of the study of inelastic diffractive processes. We demonstrate that the diffractive dissociation cross sections are increasing at asymptotic energies as ($\sigma_D \propto \ln s$, $\sigma_{DD} \propto \ln s$) while their relative contribution tends to zero ($\sigma_D/\sigma_{tot} \rightarrow 0$, $\sigma_{DD}/\sigma_{tot} \rightarrow 0$). Specifically, the cross section for the diffractive production of $N_{\frac{1}{2}^+}(1440)$ is estimated as $(\frac{1}{10} \div \frac{1}{2}) \cdot 0.6 \ln \frac{s}{1.2\text{GeV}^2}$ mb if this state is a radial excitation of a nucleon.³⁴

The effect for inclusive cross sections due to the change of the regime, from the constituent quark collision picture to that with a united single disk, was discussed

in 38, 39, 40 when definite indications about hadron cross section growth appeared. It was emphasized that the approach to the single black disk regime should change probabilities of the production of hadrons in the fragmentation region (hadrons with $x = p/p_{in} \sim 1$), for more details see also ref. 41.

The increase of the black disk radius, $R_{black} \propto 2\sqrt{\Delta\alpha'_P} \ln s$, is determined by parameters of the leading t -channel singularity, that are the pomeron intercept $\alpha(0) = 1 + \Delta$ (with $\Delta > 0$) and the pomeron trajectory slope α'_P . The s -channel unitarization of the scattering amplitude damps the strong pomeron pole singularity transforming it into a multipomeron one. Therefore, we face the intersection of problems of the gluon content of the t -channel states at ultrahigh energies and the physics of glueball states - at present the glueball states are subjects of intensive investigations, see, for example 42, 43, 44, 45 and references therein. Studies of phenomenons related to glueballs and multigluon states at small $|t|$ (or at small masses) are enlightening for understanding the confinement singularity - see the discussion in ref. 46. The large value of the mass of the soft effective gluon (and the corresponding value of the low-lying glueballs) and the slow rate of the black disk increase appear to be related phenomena.

The model is based on the hypothesis of the gluon origin of the t -channel forces, and these gluons form pomerons. Mesons (two-quark composite systems) and baryons (three-quark composite systems) scatter on the pomeron cloud. It is supposed that the pomeron cloud is materialized as a low-density gas, and pomeron-pomeron interactions, as well as t -channel transitions $P \rightarrow PP$, $P \rightarrow PPP$ and so on, can be neglected.

Consequently, the hadron-hadron scattering amplitude is determined by the set of diagrams with multiple pomeron exchanges (for πp scattering it is shown in Fig. 2a,b,c). Pion-pomeron and proton-pomeron coupling diagrams are shown in Fig. 2d-g and Fig. 2h-l. Gluon structure of pomeron provides the colour screening effect in couplings.⁴⁷

The convergence of the coupling diagrams is guaranteed by vertices $\pi \rightarrow q\bar{q}$ and $p \rightarrow qqq$, or quark wave functions of hadrons $\varphi_\pi^2(\mathbf{r}_1, \mathbf{r}_2)$ and $\varphi_p^2(\mathbf{r}_1, \mathbf{r}_2, \mathbf{r}_3)$, where \mathbf{r}_a are the transverse coordinates of quarks. Quark wave functions can be determined using the corresponding form factors, an example for such a determination is given in 48.

The shape of the black disk is formed by the t -channel pomeron exchanges: in 31, 33 it is a two-pole presentation of the QCD-motivated pomeron with intercepts $\alpha(0) = 1$ and $\alpha(0) = 1 + \Delta$. The two-pole pomeron exchange is popular from the sixties till now, see for example ref. 49. In the ultra-high energy region the leading pomeron dominates, according to fit³³ its trajectory reads:

$$\begin{aligned} \alpha_P(\mathbf{q}_\perp^2) &\simeq 1 + \Delta - \alpha'_P \mathbf{q}_\perp^2 \\ \Delta &= 0.273 \pm 0.011, \quad \alpha'_P = 0.129 \pm 0.007(\text{GeV}/c)^{-2} \end{aligned} \quad (3)$$

Meson-pomeron and baryon-pomeron couplings vanish for squeezed configurations of quarks: for mesons at $|\mathbf{r}_{12}| \rightarrow 0$ and for baryons at $|\mathbf{r}_{12}| \rightarrow 0$, $|\mathbf{r}_{13}| \rightarrow 0$

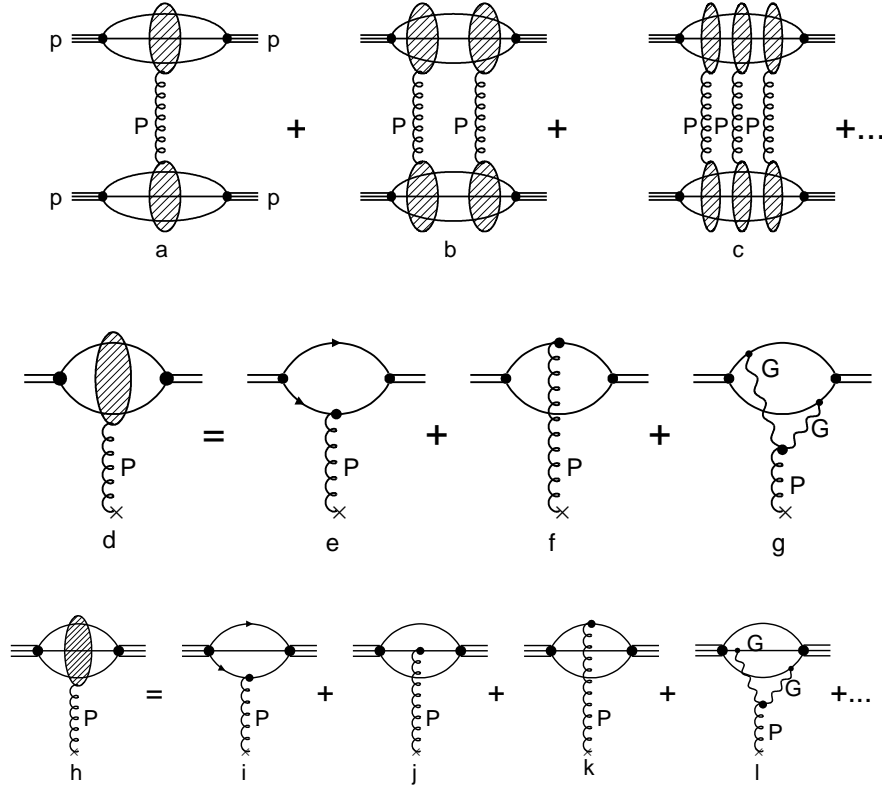


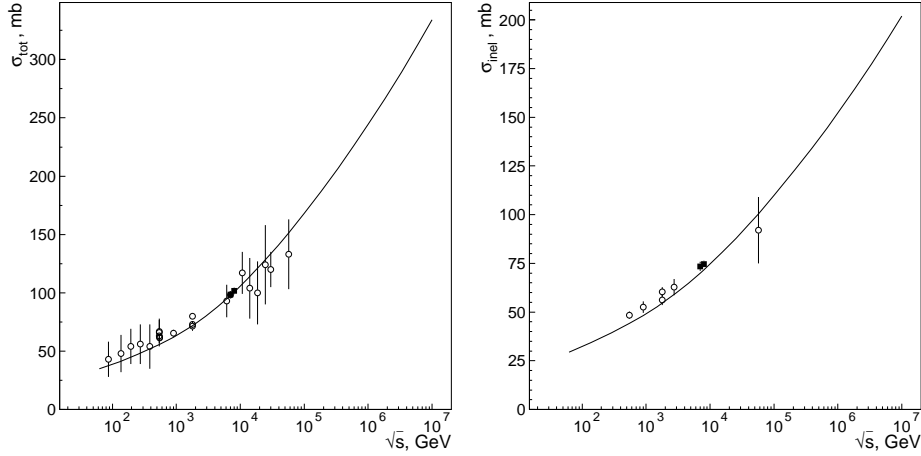
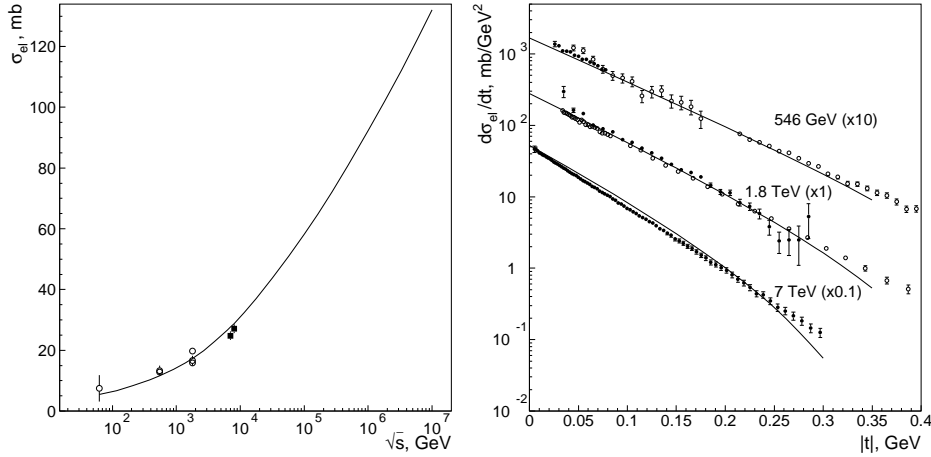
Fig. 2. Hadron-hardron collisions: (a)–(c) diagrammatic representation of the πp scattering amplitude as a set of s -channel pomeron (P) interactions; (d)–(g) pion-pomeron vertex and its deciphering: pomeron-quark terms and GGP term which describes interaction of gluons (G) of pomeron with both quarks of pion; (h)–(l) proton-pomeron vertex and corresponding P and GGP exchanges.

where $|\mathbf{r}_{ij}| = |\mathbf{r}_i - \mathbf{r}_j|$ that is a result of interplay of one-quark interaction couplings and two-quark interaction.⁴⁷ Corresponding diagrams which guarantee the colour screening are shown in Figs. 2d–g for mesons and Figs. 2h–l for baryons.

Results of description of ultrahigh energy data, that are pp data including those at LHC energies¹⁷ and cosmic ray ones,¹⁸ are demonstrated in Figs. 3,4.

In Fig. 3 we show total and inelastic cross sections, the fit gives a good approximation to data at $\sqrt{s} \sim 50 - 5 \cdot 10^4$ GeV; we also show predictions for the region $\sqrt{s} \lesssim 10^5$ GeV. The fit gives reasonably good level of description of σ_{el} and the differential cross section $d\sigma_{el}/d\mathbf{q}_\perp^2$, see Fig. 4.

The fit curves for σ_{tot} , σ_{inel} and σ_{el} look like as the LHC energy is a turning point for the cross section growth regime. Definitely it is seen when considering the scattering amplitude in the impact parameter space.


 Fig. 3. Total and inelastic cross section data^{1–5,17,18} and fit in the Dakhno-Nikonov model.

 Fig. 4. Elastic cross section and differential cross sections $d\sigma_{el}/dq_{\perp}^2$ at $\sqrt{s} = 0.546, 1.8, 7.0$ TeV and their descriptions in the fit.

2. Scattering Amplitude in the Impact Parameter Space

In Fig. 5 we show profile functions $T(b)$ determined as

$$\begin{aligned} \sigma_{tot} &= 2 \int d^2b T(b) = 2 \int d^2b \left[1 - e^{-\frac{1}{2}\chi(b)} \right], \\ 4\pi \frac{d\sigma_{el}}{dq_{\perp}^2} &= A^2(\mathbf{q}_{\perp}^2), \quad A(\mathbf{q}_{\perp}) = \int d^2b e^{i\mathbf{b}\mathbf{q}_{\perp}} T(b) \end{aligned} \quad (4)$$

The profile functions $T(b)$ at energies $0.5 - 10^3$ TeV are shown in Fig. 5a - it is seen that the profile function saturation mode, $T(b) \rightarrow 1$, works at ultra-high energies (100 – 1000 TeV), at LHC energies the saturation mode is only starting.

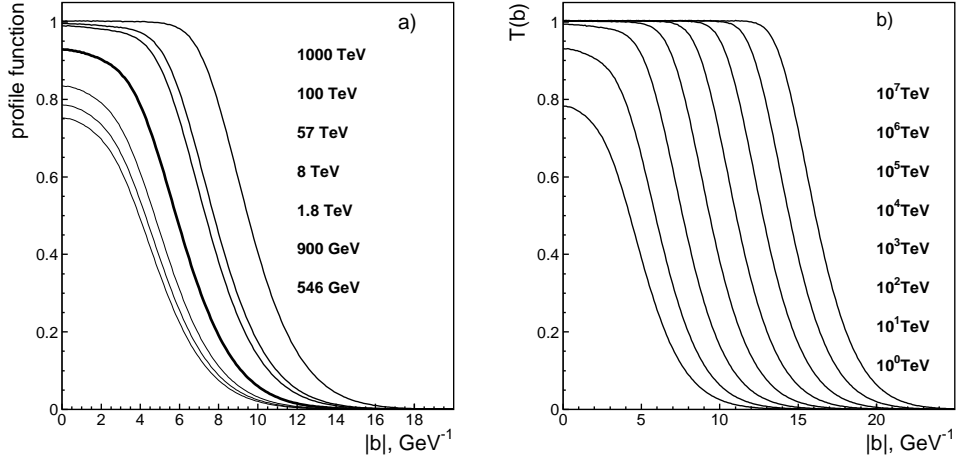


Fig. 5. a) Profile functions $T(b)$ determined in Eq. (4) at preLHC (0.546–1.8 TeV), LHC (8.0 TeV), Pierre Auger Collaboration (57 TeV) and ultra-high (100–1000 TeV) energies. b) Profile functions $T(b)$ at a set of energies $\sqrt{s} = 1, 10, 100, \dots, 10^7$ TeV.

The profile functions at 0.546 – 1.8 TeV illustrate the two-fold structure of proton, corresponding to Fig. 1d. At that energies the absorption area is dominantly inside the proper nucleon size, $b \leq 4 \text{ GeV}^{-1}$, and only the blackness level is increasing with energy.

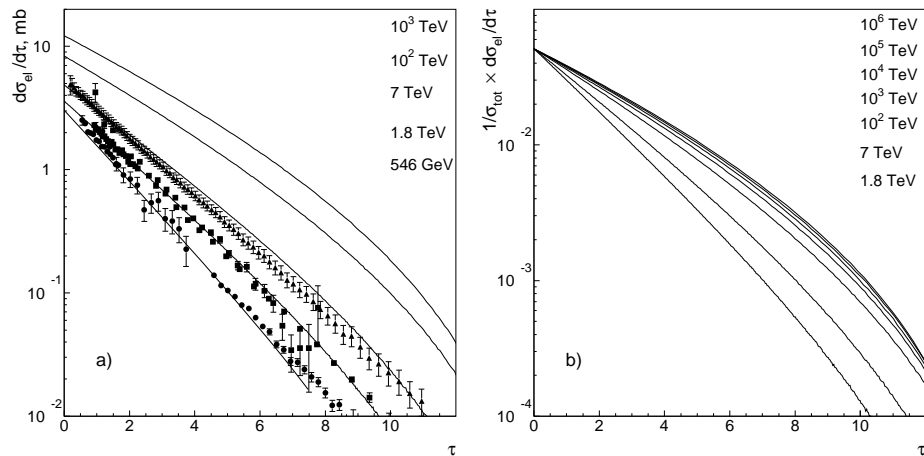


Fig. 6. a) Differential cross sections $d\sigma_{el}/d\tau$, where $\tau = \sigma_{tot} \mathbf{q}_{\perp}^2$, at $\sqrt{s} = 0.546, 1.8, 7.0$ TeV and their descriptions in the Dakhno-Nikonov model; b) Calculated differential cross sections $1/\sigma_{tot} \times d\sigma_{el}/d\tau$ at $\sqrt{s} = 1.8, 7, 100, 1000, \dots, 10^6$ TeV and their approaching to the τ -scaling limit.

3. Diffractive Cross Section and the τ -Scaling Limit

In Fig. 6a we show $d\sigma_{el}/d\tau$ with $\tau = \sigma_{tot}\mathbf{q}_\perp^2$ at ISR and LHC energies; the approach of $1/\sigma_{tot} \times d\sigma_{el}/d\tau$ to the τ -scaling limit is demonstrated in Fig. 6b. The τ -scaling, being inherent with the Dakhno-Nikonov model, works with a dimensionless object, $1/\sigma_{tot} \times d\sigma_{el}/d\tau$, in terms of the variable τ . So the scaling regime works at constrained region of non-large τ (or $\tau \leq 10$), it is the region of the diffractive cone.

The region of large τ attracts attention as well, see, for example, 14, 22, 50, 51. However, the large- τ region can be formed by next-to-leading t -channel singularities which are related to other physics, not physics of the diffractive processes.

A variable similar to τ , which also can be used for the description of the discussed diffractive distributions, $\tilde{t} = \mathbf{q}_\perp^2 \ln^2 s$, was used in 14, 22. In 22 the diffractive distribution was considered in terms of such a variable but with a dumping factor at small \tilde{t} that means strengthening the role of non-peripheral interactions of the large- τ region.

4. The Black Disk Radius and $\ln^2 s$ -Growth of Total and Elastic Cross Sections

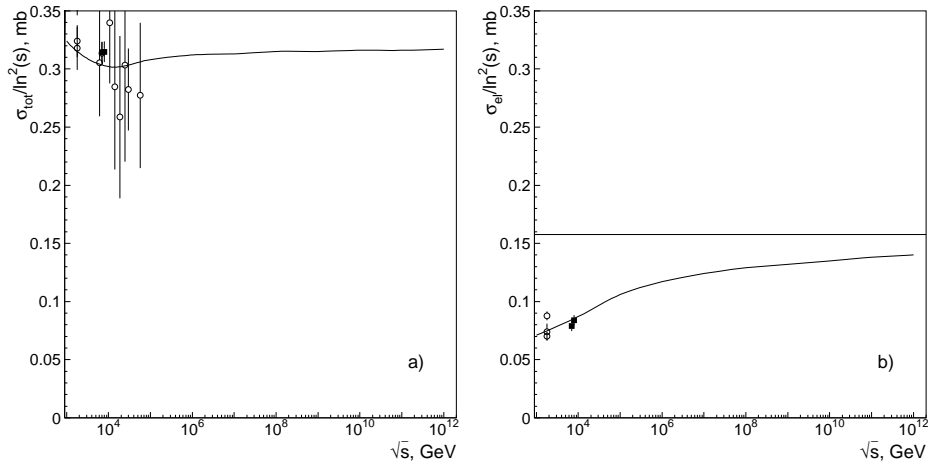


Fig. 7. Values for $\sigma_{tot}(pp)/\ln^2 s/s_0$ and $\sigma_{el}(pp)/\ln^2 s/s_0$ (where $\sqrt{s_0} = 1$ GeV) in the Dakhno-Nikonov model versus data.^{1-5, 17, 18} The straight line is the asymptotic limit for the elastic cross section: $\sigma_{el}^\infty(s)/\ln^2 s = \frac{1}{2}\sigma_{tot}^\infty/\ln^2 s$.

At $\ln s \gg 1$, when the asymptotic regime works, there are two clear regions in the b -space (Fig. 5): with $T(b) \simeq 1$ (black disk area) and $T(b) \simeq 0$ (transparent area). Conventionally we determine these areas by the constraints: $T(b) > 0.97$ and

$T(b) < 0.03$. Then

$$\begin{aligned} \mathbf{b}^2 &< 4\Delta\alpha'_P \ln^2 \frac{s}{s_-}, & \text{with } T(b) > 0.97, \\ \mathbf{b}^2 &> 4\Delta\alpha'_P \ln^2 \frac{s}{s_+}, & \text{with } T(b) < 0.03, \end{aligned} \quad (5)$$

which gives the black disk radius:

$$R_{black} = 2\sqrt{\Delta\alpha'_P} \ln \frac{s}{s_R}, \quad \sqrt{s_R} \simeq 80 \text{ GeV}, \quad (6)$$

with $s_- < s_R < s_+$. The black disk radius depends on parameters of the leading pomeron only (factor $2\sqrt{\Delta\alpha'_P} \simeq 0.08$ fm) that results in Gribov's universality of hadronic total cross sections at asymptotic energies.³⁷

An approach of $\sigma_{tot}(s)$ and $\sigma_{el}(s)$ to asymptotic values is shown on Fig. 7 - the calculations demonstrate a relatively fast appearance of asymptotics in $\sigma_{tot}(s)$ in contrast to $\sigma_{el}(s)$. A slow increase of $\sigma_{el}(s)$ means a slow approach of $\sigma_{inel}(s) = \sigma_{tot}(s) - \sigma_{el}(s)$ to the asymptotic behaviour.

5. Diffractive dissociation cross sections

The relative weight of quasi-elastic processes falls with energy growth as $1/\ln s$; this is in agreement with $\sigma_{tot}/\sigma_{el} \rightarrow 2$. In Fig. 8a we demonstrate the ratio

$$\frac{\sigma_{X(p)X(p)}(pp) - \sigma_{el}(pp)}{\sigma_{tot}(pp)} = \frac{2\sigma_{D(p)}(pp) + \sigma_{D(p)D(p)}(pp)}{\sigma_{tot}(pp)} \sim \frac{1}{\ln s}, \quad (7)$$

it tends to zero at $\ln s \rightarrow \infty$. In Fig. 8b we show the sum of the quasi-elastic cross sections $2\sigma_{D(p)}(pp) + \sigma_{D(p)D(p)}(pp)$ (solid line) and the single diffractive dissociation cross section $\sigma_{D(p)}(pp)$ (dashed line). Calculations show that the diffractive dissociation cross sections increase as follows:

$$\begin{aligned} 2\sigma_{D(p)}(pp) + \sigma_{D(p)D(p)}(pp) &= \sigma_{X(p)X(p)}(pp) - \sigma_{el}(pp) \simeq 0.58 \ln \frac{s}{104 \text{ GeV}^2} \text{ mb}, \\ \sigma_{D(p)}(pp) &= \sigma_{X(p)}(pp) - \sigma_{el}(pp) \simeq 0.25 \ln \frac{s}{1007 \text{ GeV}^2} \text{ mb}, \\ \sigma_{D(p)D(p)}(pp) &\simeq (0.08 \ln s + 0.5) \text{ mb}. \end{aligned} \quad (8)$$

s is given in GeV^2 units. At 7 TeV calculations give $2\sigma_{D(p)}(pp) + \sigma_{D(p)D(p)}(pp) \simeq 7.6$ mb $\sigma_{D(p)}(pp) \simeq 2.7$ mb. The values tell us that the single diffraction dissociation gives the main contribution to the quasi-elastic diffractive processes, while the double diffraction increases more slowly. The corresponding cross sections are related to semitransparent disk rim:

$$\begin{aligned} 2\sigma_{D(p)}(pp) + \sigma_{D(p)D(p)}(pp) &= 2\pi R_{black} \delta R(2D + DD), \\ \delta R(2D + DD) &= 0.16 \pm 0.04 \text{ fm}, \\ \sigma_{D(p)}(pp) &= 2\pi R_{black} \delta R(D), \\ \delta R(D) &= 0.06 \pm 0.01 \text{ fm}, \end{aligned} \quad (9)$$

Recall, $R_{black} \simeq 0.16 \ln(\sqrt{s}/80\text{GeV})$ fm.

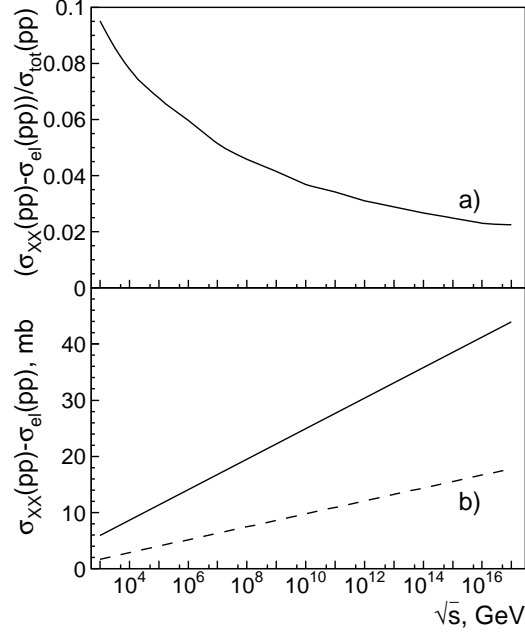


Fig. 8. Diffractive processes: a) the ratio $\left(2\sigma_{D(p)D(p)}(pp) + \sigma_{D(p)D(p)}(pp)\right) / \sigma_{tot}(pp)$ determined according to Eq. (7) and b) differences $\sigma_{X(p)X(p)}(pp) - \sigma_{el}(pp) = 2\sigma_{D(p)D(p)}(pp) + \sigma_{D(p)D(p)}(pp)$ (solid line) and $\sigma_{X(p)}(pp) - \sigma_{el}(pp) = \sigma_{D(p)}(pp)$ (dashed line), presented in Eq. (8).

6. Contribution of u -Channel and the Real Part of the Scattering Amplitude

The ratio $Re A_{el}/Im A_{el}$ at $\mathbf{q}_{\perp}^2 \simeq 0$ at asymptotic energies is determined by the analyticity of the scattering amplitude. Taking into account contributions of s and u channels we write:

$$A_{el} \propto i [\ln^2(s/s_0) + \ln^2(-s/s_0)], \quad \frac{Re A_{el}}{Im A_{el}} \simeq \frac{\pi}{\ln(s/s_{0R})}. \quad (10)$$

with $-s = se^{-i\pi}$ and $\ln^2(se^{-i\pi}) = (\ln s - i\pi)^2 \simeq \ln^2 s - 2\pi i \ln s$.

Experimental data ($Re A_{el}/Im A_{el} = 0.14_{-0.08}^{+0.0117}$) require a small value of s_{0R} . For 7 TeV Eq. (10) gives us $Re A_{el}/Im A_{el} = 0.15$ at $\sqrt{s_{0R}} = 200$ MeV that is an inverse value of the radius of a black disk at such an energy, ~ 1 fm. So, the $Re A_{el}/Im A_{el}$ is determined by the size of the disk while the rate of its growth by the leading pomeron characteristics.

The real part of the scattering amplitude at $\mathbf{q}_{\perp}^2 > 0$ can be also determined by analyticity requirement. We write

$$A_{el} = \frac{i}{2} \left[\ln^2(s/s_0)A(\tau) + \ln^2(-s/s_0)A(\tau^+) \right]. \quad (11)$$

Here $\tau = \sigma_{tot}(s)\mathbf{q}_\perp^2$ and $\tau^+ = \sigma_{tot}(-s)\mathbf{q}_\perp^2 \simeq \left(1 - \frac{2\pi i}{\ln s}\right)\sigma_{tot}(s)\mathbf{q}_\perp^2 = \left(1 - \frac{2\pi i}{\ln s}\right)\tau$. Therefore the scattering amplitude within account of the real part terms reads:

$$A_{el} \simeq i \ln^2 s \left[A(\tau) - \frac{\pi i}{\ln s} \left(A(\tau) + \tau \frac{dA(\tau)}{d\tau} \right) \right]. \quad (12)$$

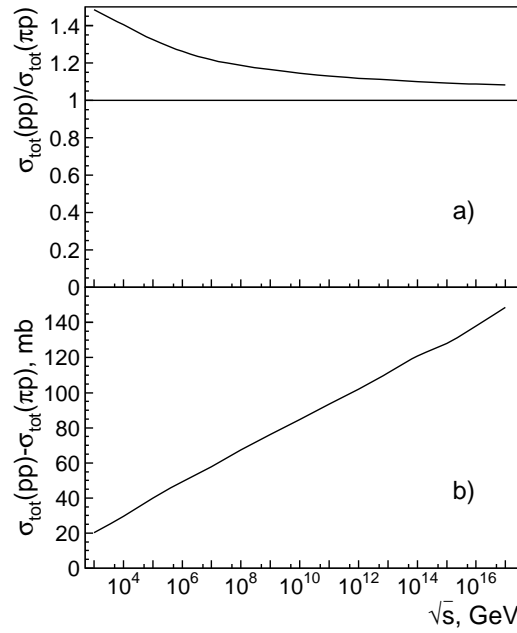


Fig. 9. a) Ratio of proton-proton and pion-proton total cross sections, $\sigma_{tot}(pp)/\sigma_{tot}(\pi p) \rightarrow 1$, and b) its difference $\sigma_{tot}(pp) - \sigma_{tot}(\pi p) \propto \ln s$.

7. The πp and $\pi\pi$ Total Cross Sections and the Gribov Universality

The Dakhno-Nikonov model made it possible to extend conventionally the scheme on πp collisions - for that additionally the quark distribution to the pion is needed only. The distribution of quarks to a pion is known, see, for example, ref. 48 that allows to give predictions.

The ratio $\sigma_{tot}(pp)/\sigma_{tot}(\pi p)$ is shown in Fig. 9a, it asymptotically tends to 1. The difference of proton-proton and pion-proton total cross sections is increasing with energy, Fig. 9b, and can be described at $\sqrt{s} \gtrsim 10^6$ GeV as

$$\sigma_{tot}(pp) - \sigma_{tot}(\pi p) \simeq 1.9 \ln \frac{s}{s_0} \text{ mb}, \quad s_0 = 0.8 \text{ GeV}^2. \quad (13)$$

The universality of the total cross sections means the equality of the leading terms

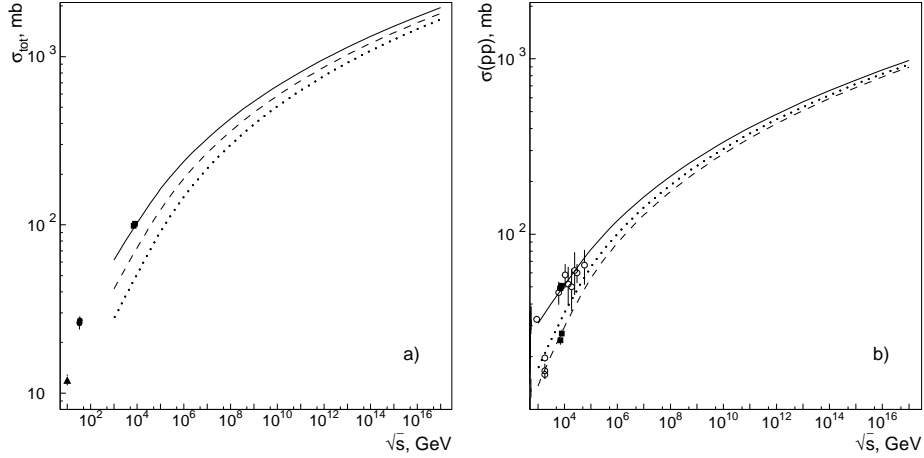


Fig. 10. a) Total cross sections: $\sigma_{tot}(pp)$ (solid line), $\sigma_{tot}(\pi p)$ (dashed line) and $\sigma_{tot}(\pi\pi)$ (dotted line). Squares (pp) are from,¹⁷ circles (πp) are from,⁵² triangles ($\pi\pi$) are from.⁵³ b) Proton-proton collisions: $\frac{1}{2}\sigma_{tot}(pp)$ (solid line), $\sigma_{el}(pp) + 2\sigma_{pD}(pp)$ (dotted line) and $\sigma_{el}(pp)$ (dashed line). Data^{1-5, 17, 18} stand for $\frac{1}{2}\sigma_{tot}(pp)$ and $\sigma_{el}(pp)$.

($\propto \ln^2 s$) only, and it is demonstrated in Fig. 10a where $\sigma_{tot}(pp)$, $\sigma_{tot}(\pi p)$ and $\sigma_{tot}(\pi\pi)$ are shown.

8. Conclusion

The twofold structure of hadrons – hadrons are built by constituent quarks and the latter are formed by clouds of partons – manifests itself in hadron collisions. At moderately high energies colliding protons reveal themselves in the impact parameter space as three disks corresponding to three constituent quarks, Fig. 1a. At ultra-high energies the situation is transformed to a one-disk picture, Fig. 1c, and the energy of this transformation is that of LHC. The radius of the black disk at asymptotic energies is increasing, $R_{\text{black}} \simeq 2\sqrt{\Delta\alpha'_p} \ln s$, that provides a $\ln^2 s$ growth of total and elastic cross sections $\sigma_{tot} \simeq 2\pi R_{\text{black}}^2$ and $\sigma_{el} \simeq \pi R_{\text{black}}^2$. Diffractive dissociation cross sections are increasing as $\ln s$ being related to the black disk rim effect: $\sigma_D \propto 2\pi R_{\text{black}}$ and $\sigma_{DD} \propto 2\pi R_{\text{black}}$.

A steady increase of the black disk radius R_{black} , is determined by parameters of the leading t -channel singularity only: that are the pomeron intercept $\alpha(0) = 1 + \Delta$ ($\Delta > 0$) and the pomeron trajectory slope α'_p . The s -channel unitarization of the scattering amplitude damps the strong pomeron pole singularity transforming it into a multipomeron one. Therefore, we face the intersection of problems of the gluon content of the t -channel states at ultrahigh energies and the physics of gluonic states, glueballs. At present the glueball states are subjects of intensive investigations, see, for example 42, 43, 45 and references therein. Studies of phenomena related to glueballs and multigluon states at small $|t|$ are enlightening for the confinement

singularity problem - see discussion in ref. 46. The large value of mass of the soft effective gluon (and the corresponding values of the low-lying glueballs) and the slow rate of the black disk increase appear to be closely related phenomena.

The change of the regime, from the constituent quark collision picture to that with a united single disk, was discussed in 38, 39, 40 when definite indications about the hadron cross section growth appears. It was emphasized that the single black disk regime should change probabilities of productions of hadrons in the fragmentation region (hadrons with $x = p/p_{in} \sim 1$), for more detailed discussion see 41.

Acknowledgment

We thank Ya.I. Azimov, M.G. Ryskin, and A.V. Sarantsev for useful discussions and comments. The work was supported by grants RFBR-13-02-00425 and RSGSS-4801.2012.2.

References

1. UA4 Collaboration, Phys. Lett. **B147** (1984) 385.
2. UA4/2 Collaboration, Phys. Lett. **B316** (1993) 448.
3. UA1 Collaboration, Phys. Lett. **B128** (1982) 336.
4. E710 Collaboration, Phys. Lett. **B247** (1990) 127.
5. CDF Collaboration, Phys. Rev. **D50** (1994) 5518.
6. M. Froissart, Phys. Rev. **123** (1961) 1053.
7. A.B. Kaidalov and K.A. Ter-Martirosyan, Sov. J. Nucl. Phys. **39** (1984) 979.
8. A. Donnachie and P.V. Landshoff, Nucl. Phys. **B231** (1984) 189.
9. R.J. Glauber, Phys. Rev. **100** (1955) 242.
10. R.J. Glauber, *Lectures in Theoretical Physics*, ed. W.E. Britten, L.G. Danham, Vol.1, New York (1959) 315.
11. T.K. Gaisser and T. Stanev, Phys. Lett., **B219** (1989) 375.
12. M. Block, F. Halzen and B. Margolis, Phys. Lett., **B252** (1990) 481.
13. R.S. Fletcher, Phys. Rev. **D46** (1992) 187.
14. Y.I. Azimov, Phys. Rev. **D84**, 056012 (2011); arXiv:1208.4304.
15. ATLAS collaboration, Nature Commun. **2** (2011) 463.
16. CMS collaboration, Phys. Lett. **B722** (2013) 5.
17. G. Latino for the TOTEM collaboration, *Summary of Physics Results from the TOTEM Experiment*, arXiv:1302.2098.
18. Pierre Auger Collaboration (P. Abreu et al.), Phys. Rev. Lett. **109** (2012) 062002.
19. V.A. Schegelsky, M.G. Ryskin, Phys. Rev. **D85**, (2012) 094024.
20. M.M. Block and F. Halzen, Phys. Rev. **D86** (2012) 051504.
21. M.G. Ryskin, A.D. Martin and V.A. Khoze, Eur. Phys. J. **C72** (2012) 1937.
22. I.M. Dremin and A.A. Radovskaya, Europhys. Lett. **100** (2012) 61001.
23. E. Martynov, Phys. Rev. **D87** (2013) 114018.
24. M. Ryskin, A. Martin, and V. Khoze, Eur.Phys.J. **C60** (2009) 249.
25. M. Ryskin, A. Martin, and V. Khoze, Eur.Phys.J. **C71** (2011) 1617.
26. V. Khoze, A. Martin, and M. Ryskin, Eur.Phys.J. **C73** (2013) 2503.
27. V. Khoze, A. Martin, and M. Ryskin, arXiv:1312.3851.
28. U. Maor, arXiv:1310.7340.
29. E. Gotsman, arXiv:1304.7627.

30. S. Ostapchenko, Phys.Rev. **D81** (2010) 114028.
31. L.G. Dakhno and V.A. Nikonov, Eur. Phys. J. **A8** (1999) 209.
32. M.L. Good, W.D. Walker, Phys. Rev. **120** (1960) 1857.
33. V.V. Anisovich, K.V. Nikonov and V.A. Nikonov, Phys. Rev. **D88** (2013) 014039.
34. V.V. Anisovich, V.A. Nikonov and J. Nyiri Phys. Rev. **D88** (2013) 094015.
35. M.M. Block and F. Halzen, arXiv:1210.4086v1.
36. M.J. Menon and P.V.R.G. Silva, arXiv:1212.5096v1.
37. V.N. Gribov, Yad. Fiz. **17** (1973) 603, [Sov. J. Nucl. Phys. **17** (1973) 313].
38. V.V. Anisovich and V.M. Shekhter, Yad. Fiz. **28** (1978) 1079, [Sov. J. Nucl. Phys. **28** (1978) 554].
39. V.V. Anisovich, E.M. Levin and M.G. Ryskin, Yad. Fiz. **29**, 1311 (1979), [Sov. J. Nucl. Phys. **29**, 674 (1979)].
40. V.V. Anisovich, V.M. Braun and Yu.M. Shabelski, Yad. Fiz. **36** (1982) 1556, [Sov. J. Nucl. Phys. **36** (1982) 904].
41. V.V. Anisovich, M.N. Kobrinsky, J. Nyiri, Yu.M. Shabelski, *Quark model and high energy collisions*, Second Edition, World Scientific, Singapore (2004).
42. V.V. Anisovich, Usp. Fiz. Nauk **47** (2004) 45 [Phys. Usp. **47** (2004) 45].
43. A.V. Anisovich, V.V. Anisovich, M.A. Matveev, V.A. Nikonov, J. Nyiri, A.V. Sarantsev, *Mesons and Baryons. Systematization and Methods of Analysis*, World Scientific, Singapore (2004).
44. E. Klempt and A. Zaitsev, Phys. Rept. **454** (2007) 1.
45. W. Ochs, J. Phys. **40** (2013) 043001.
46. A.V. Anisovich, V.A. Nikonov, A.V. Sarantsev, V.V. Anisovich, M.A. Matveev, T.O. Vulf, J. Nyiri, Phys. Rev. **D84** (2011) 076001.
47. V.V. Anisovich, L.G. Dakhno, and V.A. Nikonov, Phys. Rev. **D44**, 1385 (1991).
48. V.V. Anisovich, D.I. Melikhov, and V.A. Nikonov, Phys. Rev. **D52** (1995) 5295.
49. A. Donnachie and P.V. Landshoff, arXiv:11122485, arXiv:1309.1292.
50. V. Uzhinsky and A. Galoyan, arXiv:1111.4984v5.
51. I.M. Dremin, Nucl. Phys. **A888** (2012) 1.
52. U. Dersch *et al.* [SELEX Collaboration], Nucl. Phys. **B579** (2000) 277.
53. H. Abramowicz, M. Gorski, G. Sinapius, A. Wroblewski, A. Zieminski, H. J. Lubatti, K. Moriyasu and C. D. Rees *et al.*, Nucl. Phys. **B 166** (1980) 62.